



Distant coupling between RNA editing and alternative splicing of the osmosensitive cation channel *Tmem63b*

Received for publication, September 16, 2020, and in revised form, October 17, 2020. Published, Papers in Press, October 25, 2020, DOI 10.1074/jbc.RA120.016049

Dan Wu^{1,2,‡}, Yan-Yu Zang^{1,2,‡}, Yong-Yun Shi^{3,‡}, Chang Ye^{1,2}, Wen-Min Cai^{1,2}, Xiao-Hui Tang^{4,5}, Liyun Zhao⁶, Yong Liu⁷, Zhenji Gan^{1,2}, Gui-quan Chen^{1,2,8}, Yun Xu^{2,8}, Jian-Jun Yang^{4,*}, and Yun Stone Shi^{1,2,8,9,*}

From the ¹Ministry of Education Key Laboratory of Model Animal for Disease Study, Model Animal Research Center, Medical School, Nanjing University, Nanjing, China, the ²State Key Laboratory of Pharmaceutical Biotechnology, Department of Neurology, Affiliated Drum Tower Hospital of Nanjing University Medical School, Nanjing University, Nanjing, China, the ³Department of Orthopaedics, Luhe People's Hospital Affiliated to Yangzhou University, Nanjing, China, the ⁴Department of Anesthesiology and Perioperative Medicine, First Affiliated Hospital of Zhengzhou University, Zhengzhou, China, the ⁵School of Medicine, Southeast University, Nanjing, China, the ⁶Translational Science and Clinical Biomarker, BeiGene (Shanghai) Co., Ltd., Shanghai, China, the ⁷Hubei Key Laboratory of Cell Homeostasis, College of Life Sciences, Institute for Advanced Studies, Wuhan University, Wuhan, China, the ⁸Institute for Brain Sciences, Nanjing University, Nanjing, China, and the ⁹Chemistry and Biomedicine Innovation Center, Nanjing University, Nanjing, China

Edited by Ronald C. Wek

Post-transcriptional modifications of pre-mRNAs expand the diversity of proteomes in higher eukaryotes. In the brain, these modifications diversify the functional output of many critical neuronal signal molecules. In this study, we identified a brain-specific A-to-I RNA editing that changed glutamine to arginine (Q/R) at exon 20 and an alternative splicing of exon 4 in *Tmem63b*, which encodes a ubiquitously expressed osmosensitive cation channel. The channel isoforms lacking exon 4 occurred in ~80% of *Tmem63b* mRNAs in the brain but were not detected in other tissues, suggesting a brain-specific splicing. We found that the Q/R editing was catalyzed by Adar2 (Adarb1) and required an editing site complementary sequence located in the proximal 5' end of intron 20. Moreover, the Q/R editing was almost exclusively identified in the splicing isoform lacking exon 4, indicating a coupling between the editing and the splicing. Elimination of the Q/R editing in brain-specific *Adar2* knockout mice did not affect the splicing efficiency of exon 4. Furthermore, transfection with the splicing isoform containing exon 4 suppressed the Q/R editing in primary cultured cerebellar granule neurons. Thus, our study revealed a coupling between an RNA editing and a distant alternative splicing in the *Tmem63b* pre-mRNA, in which the splicing plays a dominant role. Finally, physiological analysis showed that the splicing and the editing coordinately regulate Ca²⁺ permeability and osmosensitivity of channel proteins, which may contribute to their functions in the brain.

RNA editing is a post-transcriptional modification of pre-mRNAs that can introduce codon changes in mature mRNAs. The A (adenosine)-to-I (inosine) deamination in pre-mRNAs is the most abundant RNA editing in mammals (1). Because inosine in mRNA is interpreted as guanosine (G) during translation (2), the A-to-I editing often leads to changes in amino acid sequence. The A-to-I editing occurs in important signal mole-

cules, including α -amino-3-hydroxy-5-methyl-4-isoxazolepropionic acid receptor GluA2 subunit (3), kainate receptor GluK1 and GluK2 subunits (4), Kv1.1 α subunit, and 5-HT_{2C} receptors (5, 6), which are known to regulate neuronal development, circuit formation, neuronal degeneration, and synaptic transmission (7–10). The A-to-I editing is catalyzed by Adar (adenosine deaminases acting on RNA) enzymes, which recognize the dsRNA hairpin structure formed by the editing region and the editing site complementary sequence (ECS) and deaminate the targeted adenosine to inosine (11). In mammals, Adar1 (Adar) and Adar2 (Adarb1) catalyze deamination, whereas Adar3 (Adarb2) has no enzyme activity (1).

Alternative splicing is another type of post-transcriptional modification of pre-mRNAs in eukaryotes (12). Whereas more than 95% of genes undergo alternative splicing in human, around 63% do so in mouse (13, 14). Aberrant alternative splicing is widely observed in various diseases including Mediterranean anemia (15), Alzheimer's disease (16, 17), spinal muscular atrophy (18), ALS (19, 20), and cancers (21). Intriguingly, the A-to-I RNA editing in exons and the alternative splicing of nearby introns are often coupled. For instance, the R/G editing at exon 13 of *Gria2* regulates alternative splicing of exon 14 (flop) and exon 15 (flip) (22–24). The splicing efficiency also regulates nearby upstream editing when it is guided by intronic ECS (25, 26).

We have recently found that *Tmem63b* serves as an osmosensor in the inner ear and is required for survival of outer hair cells and hearing (27). To expand our understanding of *Tmem63b* functions in other systems, we cloned *Tmem63b* mRNA from mouse brain in the current study. We identified four isoforms of *Tmem63b* resulting from an A-to-I RNA editing that changes glutamine to arginine at exon 20 and an alternative splicing of exon 4. The editing was almost exclusively detected in the spliced isoform lacking exon 4, suggesting a linkage between the two post-transcriptional events. Using *Adar2* cKO mice and cultured cerebellar granule neurons (CGNs), we found that the isoform containing exon 4 suppressed the Q/R editing efficiency in a *cis* manner. Functional

This article contains supporting information.

[‡]These authors contributed equally to this work.

*For correspondence: Yun Stone Shi, yunshi@nju.edu.cn; Jian-Jun Yang, yjyangjj@126.com.

This is an Open Access article under the [CC BY](https://creativecommons.org/licenses/by/4.0/) license.

A splicing regulates a remote editing in *Tmem63b*

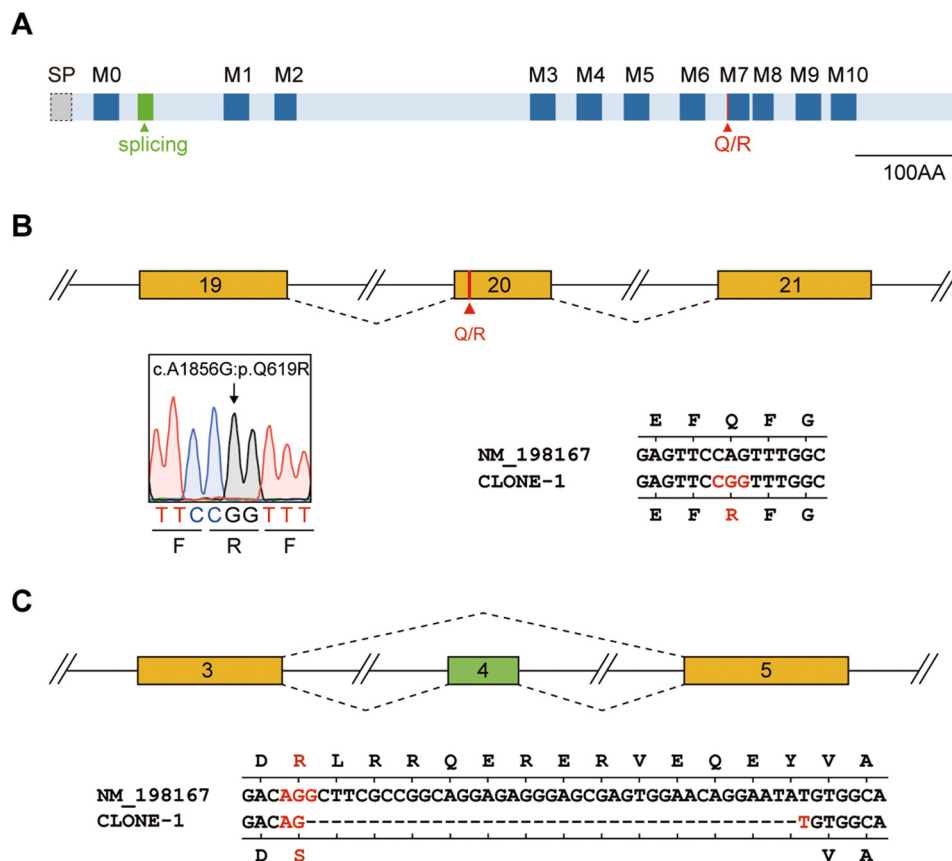


Figure 1. Q/R editing site at exon 20 and alternative splicing of exon 4 in *Tmem63b* pre-mRNA. A, domain structure of the mouse *Tmem63b* protein. The transmembrane domains (M0 to M10) are depicted in blue with linking regions in light blue. The A-to-I editing (red line) is at the intracellular linker adjacent to M7. The alternative splicing exon 4 (green block) encodes amino acids in the first intracellular loop. SP, signal peptide. Scale bar, the size of the line diagram. B, schematic representation of Q/R editing site at exon 20. Lower-left shows the sequence of the Q/R site cloned from mouse brain cDNA. Lower-right shows the cloned sequence (CLONE-1) compared with documented *Tmem63b* mRNA sequence NM_198167. The corresponding amino acids are shown above and under the nucleotide sequences. C, schematic representation of *Tmem63b* exons 3–5. The comparison between cloned sequence (CLONE-1) and documented *Tmem63b* sequence is shown below. The corresponding amino acids are shown above and under the nucleotide sequences.

analysis demonstrated that the splicing and the editing coordinately regulated hypoosmolarity-induced Ca^{2+} influx. Together, these results reveal a long-distance coupling between alternative RNA splicing and RNA editing in *Tmem63b*, in which the splicing plays a dominant role. These post-transcriptional modifications may enable the osmosensitive *Tmem63b* channel to play diversified roles in the brain.

Results

Q/R editing at exon 20 and alternative splicing of exon 4 in *Tmem63b* cDNAs

Recently, the osmosensitive cation channels in TMEM63 family have attracted research interests (27–29). When analyzing *Tmem63b* cDNAs from mouse brain tissues, we obtained one cDNA sequence that was different from the documented mRNA sequence NM_198167 in the NCBI database (Fig. 1A). The nucleotide c.1856 in this cDNA was guanosine, instead of the published adenine at the same site in exon 20. This finding suggested an A-to-I RNA editing that results in the substitution of glutamine codon CAG to arginine codon CGG at position 619 of the protein sequence (Fig. 1B). In addition, exon 4 was spliced out in the cDNA (Fig. 1C). Thus, the *Tmem63b* tran-

script we obtained was a new isoform with two post-transcriptional modifications, *i.e.* A-to-I editing at c.1856 in exon 20 and alternative splicing of exon 4.

Q/R editing of *Tmem63b* varies with brain regions and ages

The conversion of A to G at the 1856 site creates an endonuclease site for BsaWI (Fig. 2A). Specific primer pairs were designed to amplify sequences containing the editing site from mouse genomic DNAs (311 bp) and brain cDNAs (327 bp) (Fig. 2A). The majority of PCR products amplified from brain cDNAs of adult mice were digested by BsaWI and showed two additional bands (208 bp and 119 bp), whereas the PCR products amplified from mouse genomic DNAs were not recognized by BsaWI (Fig. 2B). BsaWI failed to digest *Tmem63b* cDNA fragments from tissues other than brain, including lung, kidney, heart, liver, and spleen (Fig. 2E), suggesting that this editing is brain-specific. In addition, the editing efficiency varied in brain sub-regions, from ~40% in the hypothalamus to ~60% in other brain regions in adult mice (Fig. 2D and Fig. S1, A and C). To investigate whether such editing was affected during the development, we examined the Q/R editing in P7 and embryonic (E12.5 and E18.5) brains and observed lower editing efficiency as compared with the adult brains (Fig. 2C and

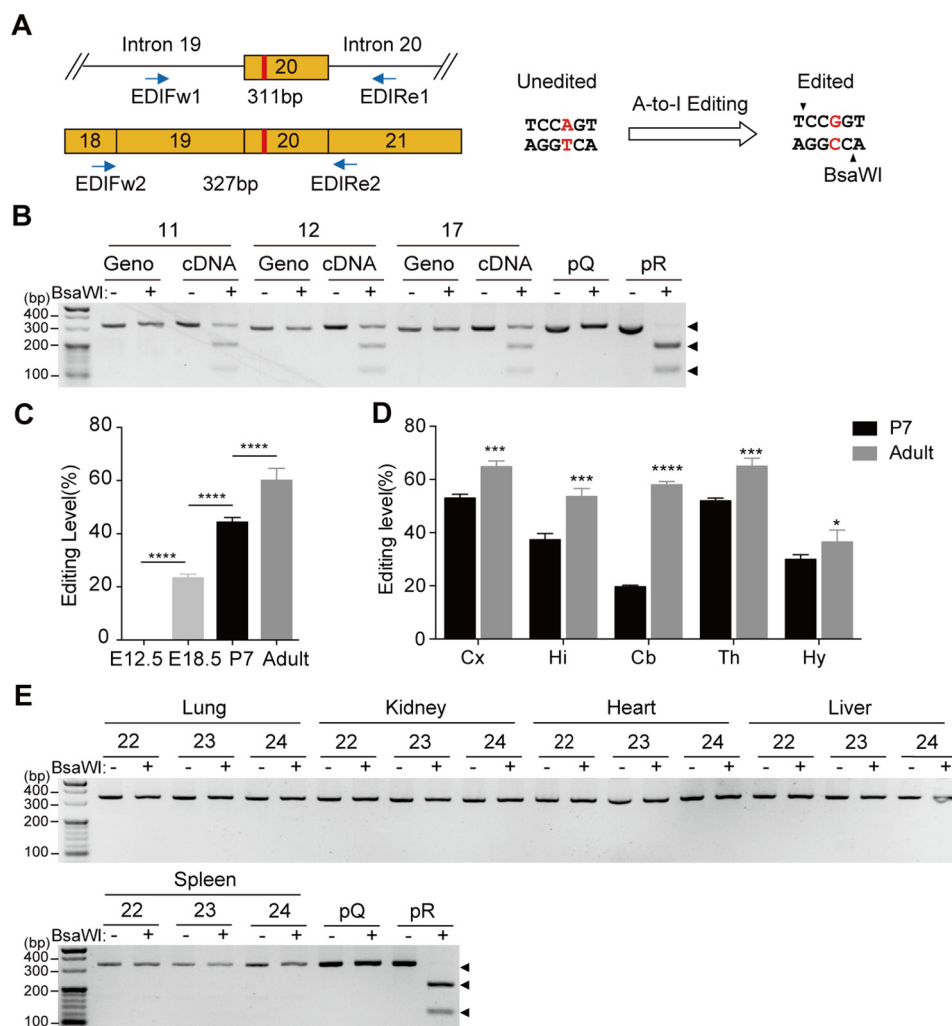


Figure 2. The brain-specific Q/R editing of *Tmem63b* varies with brain regions and ages. *A*, schematic demonstration of genomic (upper panel) and cDNA (lower panel) sequence around *Tmem63b* exon 20 with Q/R editing site marked in red. Primers for amplification are indicated. Q/R editing led to a BsaWI endonuclease recognizing site (right panel). *B*, Q/R editing of *Tmem63b* in brains of three adult mice with codes labeled above. The amplified sequences with unedited (Q) and edited (R) forms were indicated by black arrowheads. Plasmids with Q-form (pQ) and R-form (pR) *Tmem63b* cDNAs served as control to indicate the enzymatic activity of BsaWI. *C*, quantification of Q/R editing levels in brains of E12.5 (0.0 ± 0.0%, *n* = 3), E18.5 (23.7 ± 1.2%, *n* = 3), P7 (44.6 ± 1.5%, *n* = 5), and adult (60.3 ± 4.2%; *n* = 6) mice. Data are shown as mean ± S.D. (error bars). *****p* < 0.0001; one-way ANOVA, Tukey's post hoc test. *D*, quantification of Q/R editing levels in cerebral cortex (Cx), hippocampus (Hi), cerebellum (Cb), thalamus (Th), and hypothalamus (Hy) of P7 (black column) and adult (gray column) mice. Data are shown in Table S1 as mean ± S.D. **p* < 0.05; ***p* < 0.001; *****p* < 0.0001; Student's *t* test, two-tailed. *E*, Q/R editing of *Tmem63b* was absent in lungs, kidneys, hearts, livers, and spleens from three adult mice with codes labeled above.

Fig. S1, B and D). There was virtually no editing in the brains of E12.5 mice, likely because of low expression level of Adar enzymes at this stage (1). Results from different brain regions at P7 were similarly lower than those in the adult brain (Fig. 2D and Fig. S1, A and C).

Q/R editing of *Tmem63b* is catalyzed by Adar2

In mammals, Adar1 (Adar) and Adar2 (Adarb1) catalyze A-to-I editing. To determine whether Adar1 or Adar2 catalyzed the Q/R editing in *Tmem63b*, we transfected mouse Adar1 or Adar2 cDNA together with a *Tmem63b* minigene containing the genomic sequence from exon 19 to exon 21 (the editing segment) in HEK293 cells and evaluated the editing efficiency (Fig. 3A). To avoid putative contamination from endogenous *Tmem63b* in HEK cells, the exogenous RNAs were reverse-transcribed into cDNAs by a primer

RT_{IRES} (Internal Ribosome Entry Site) paired to vector sequence (Fig. 3A). Adar2 but not Adar1 transfection resulted in partial digestion of PCR products (403 bp) into two bands (284 bp and 119 bp) by BsaWI (Fig. 3B). To verify that the transfected Adar1 was functional, we coexpressed Adar1 with an *Htr2c* minigene containing the "A" editing site at exon 5 that is preferentially edited by Adar1 (30) and found that this site was efficiently edited (Fig. S2). To examine whether the *Tmem63b* Q/R editing was catalyzed by Adar2 *in vivo*, we generated Adar2 floxed mice (*Adar2^{f/f}*) and bred them with *Nestin-cre* line (31) to obtain brain-specific Adar2 cKO (*Adar2^{f/f}; Nestin-Cre*) mice (Fig. 3C). The Adar2 cKO mice were postnatally lethal, likely because of inability to edit the *Gria2* Q/R site (32). We therefore analyzed the Q/R editing of *Tmem63b* in P0 mouse brains. The Q/R editing of *Tmem63b* was completely eliminated in Adar2 cKO brains (Fig. 3, D and E).

A splicing regulates a remote editing in *Tmem63b*

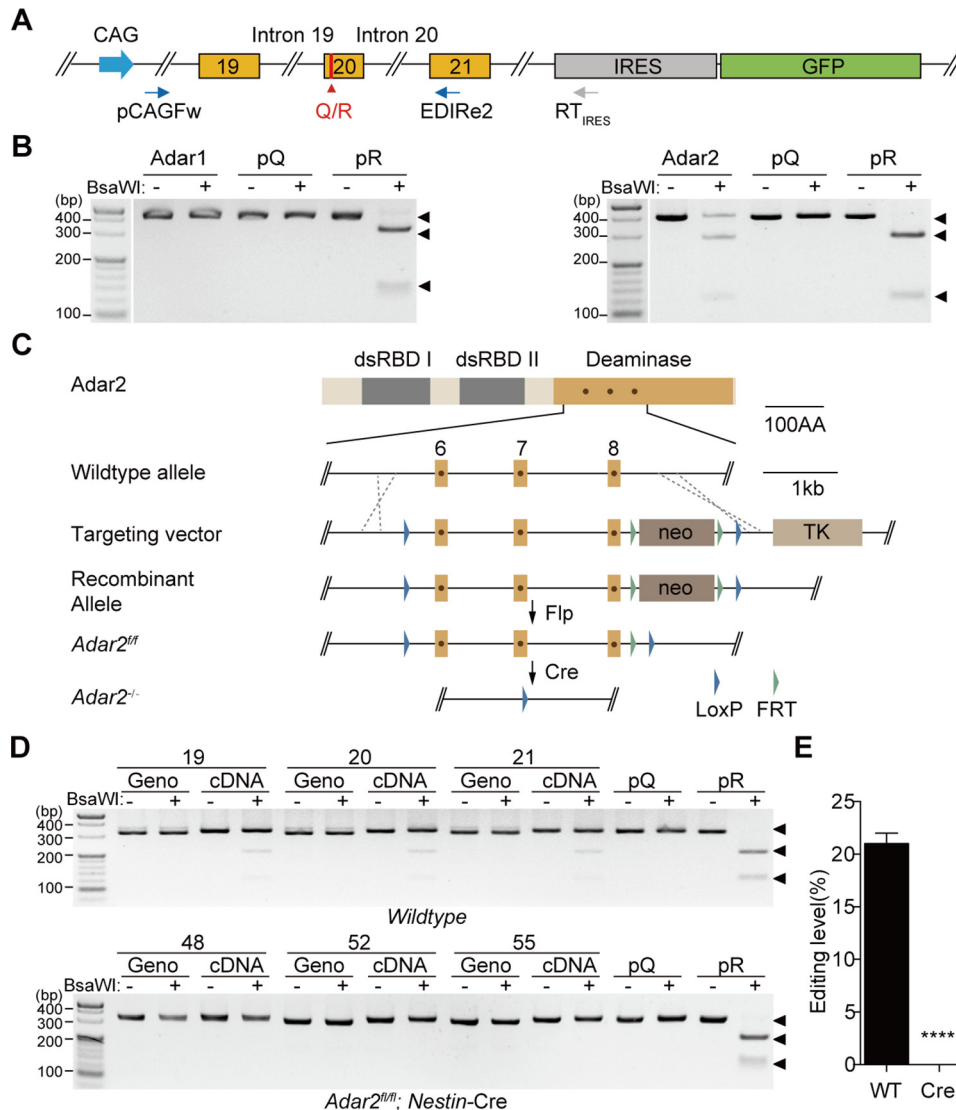


Figure 3. Q/R editing of *Tmem63b* is catalyzed by Adar2. *A*, schematic representation of the minigene construct containing the editing segment of *Tmem63b*. The minigene was driven by CAG promoter and linked with GFP through IRES. pCAGFw and EDIRe2 are primers for amplification. *B*, Q/R editing of *Tmem63b* minigene in HEK293 cells expressing Adar1 or Adar2. *C*, the generation of Adar2 floxed (*Adar2^{fl/fl}*) mice by homologous recombination techniques. The dots within the targeted exons indicate the three amino acid residues essential for the deaminase activity. dsRBD, dsRNA binding domains. TK, thymidine kinase. neo, neomycin. *D*, Q/R editing in brains from WT and brain-specific Adar2 knockout P0 mice. The experiments were repeated in three WT mice (labeled as 19, 20, and 21) and three Adar2 cKO mice (labeled as 48, 52, and 55). *E*, quantification of the Q/R editing levels in brains from WT mice ($21.0 \pm 1.0\%$, $n = 3$) and brain-specific Adar2 knockout mice ($0.0 \pm 0.0\%$, $n = 3$). Data are shown as mean \pm S.D. (error bars). **** $p < 0.0001$; Student's *t* test, two-tailed. FRT, Flp recognition target.

Analysis of the downstream ECS

To dissect the critical ECS for Q/R editing of *Tmem63b*, we analyzed the secondary structure of RNA sequence surrounding editing site using the bioinformatics software RNAstructure (33). A dsRNA duplex containing Q/R editing site was obtained, and the sequence base-paired to the editing region was predicted as ECS (in red frame, Fig. 4A). We then introduced a series of mutations on the predicted ECS and analyzed their effects on Q/R editing in Adar2 coexpressed HEK 293 cells. The editing efficiency in WT sequence was 62%, whereas deletion of 14 consecutive nucleotides from the center of ECS abolished Q/R editing (*Mut 1*, Fig. 4B). In addition, mutations on single or multiple nucleotides that destabilized the dsRNA duplex also decreased the editing efficiency (*Mut 2–Mut 9*, Fig. 4B), whereas introduction of the compensatory mutations around the editing site restored

the editing efficiency (*Mut 10–Mut 12*, Fig. 4C), indicating the importance of the hairpin structure formed by the intronic ECS and the exonic editing region. Taken together, the intronic sequence at the proximal 5' end of intron 20 was demonstrated to be the ECS for *Tmem63b* Q/R editing.

Alternative splicing of exon 4 is brain-specific

To study alternative splicing of exon 4, a pair of primers, SPFw and SPRe, were designed to amplify the sequence around exon 4 (Fig. 5A). *Tmem63b* cDNAs with (long-form) or without (short-form) exon 4 were amplified into PCR products of different lengths, 223 bp and 184 bp, respectively. The efficiency of the splicing was calculated as the percentage of short form to total *Tmem63b*. The short form was detected in brain of adult mouse but not in lung, kidney, liver, and spleen (Fig. 5B).

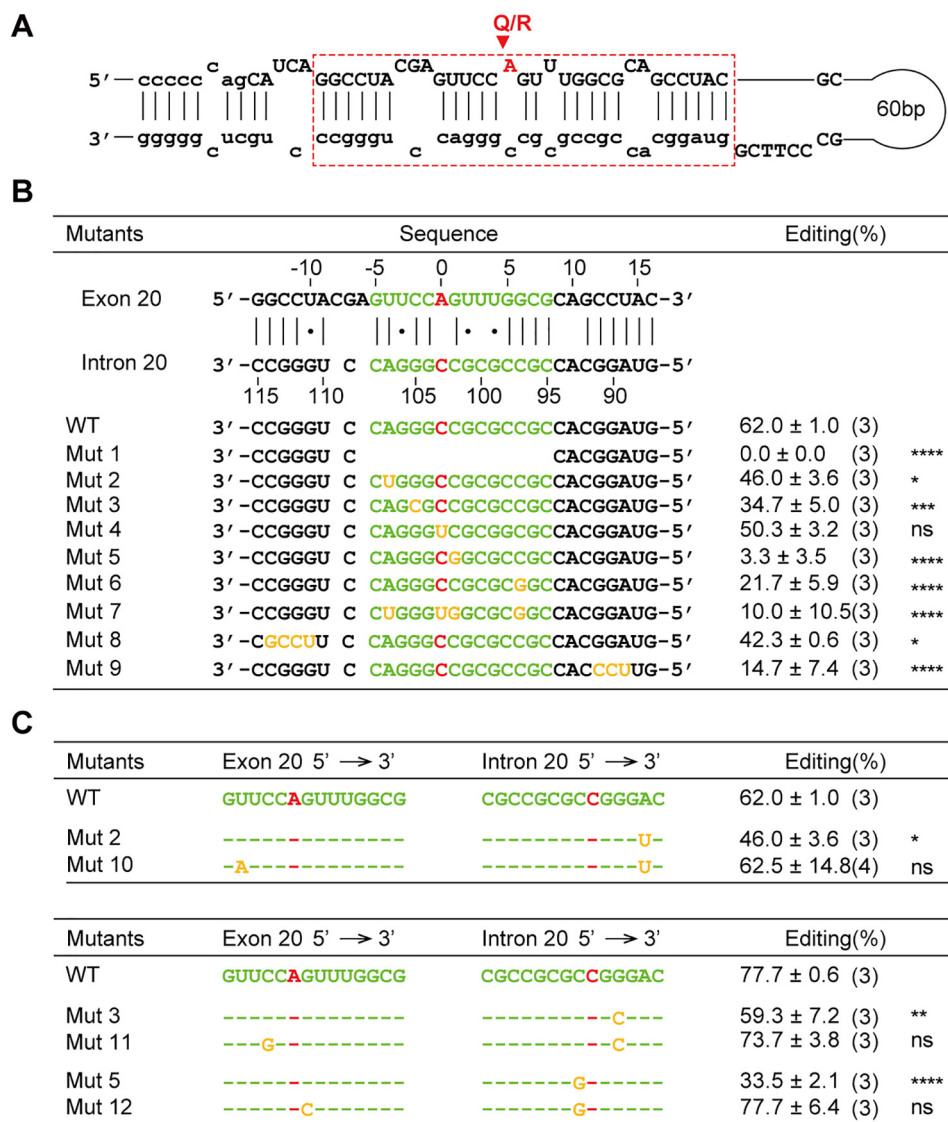


Figure 4. Analysis of downstream ECS essential for Q/R Editing. A, schematic representation of dsRNA hairpin structure formed by the editing region and the ECS, with the ECS marked in red frame and Q/R editing site in red arrowhead. B, Q/R editing of *Tmem63b* minigenes with mutations on ECS. The extent of Q/R editing was determined as illustrated in Fig. 3A. C, compensatory mutations in the editing region rescue editing efficiency impaired by mutations in ECS. The editing efficiency was quantified by measuring the peak heights ratio at the Q/R site obtained from sequencing chromatograms in the lower table. Data are shown as mean ± S.D. * $p < 0.05$; ** $p < 0.01$; *** $p < 0.001$; **** $p < 0.0001$; ns, not significant; one-way ANOVA, Tukey's post hoc test. The sample numbers of replicates are listed in parentheses.

Notably, a weak splicing occurred in about 2% of total heart *Tmem63b* mRNAs. In the whole brains, ~80% of the *Tmem63b* mRNAs were the short form. The splicing efficiency in different brain regions mildly varied from 70 to 80% (Fig. 5D and Fig. S3, A and C). In addition, the splicing efficiency in P7 mouse brains was similar to that in the adult brains, but it was modestly lower in the embryonic brains (E12.5 and E18.5), with the short form accounting for 68% of *Tmem63b* mRNAs at E12.5. These data demonstrated that the splicing efficiency in *Tmem63b* pre-mRNA was relatively stable during development (Fig. 5, B and C and Fig. S3, B and D).

Above data suggested that up to ~80% of *Tmem63b* mRNAs from mouse brain were short isoforms lacking exon 4. One concern was that the PCR reaction using this pair of primers could prefer one isoform over the other. To perform an independent evaluation on the splicing efficiency, we designed three

pairs of primers to amplify the short form, the long form, and the total *Tmem63b* mRNAs, respectively, and examined the splicing by quantitative real-time PCR (Fig. 5E). The results showed that the long form (exon 3-4-5) and the short form (exon 3-5) were 18.7% and 77.5%, respectively, of the total *Tmem63b* mRNAs (exon 5) (Fig. 5E). This experiment further verified that around 80% of mRNAs from adult mouse brain were short isoforms. Taken together, the alternative splicing of *Tmem63b* exon 4 is brain-specific. The splicing efficiency is constant among different brain regions and relatively stable at different development stages.

Distant coupling between alternative splicing and editing in *Tmem63b*

Previous studies demonstrated that A-to-I editing in exons and splicing of nearby downstream introns could affect each

A splicing regulates a remote editing in *Tmem63b*

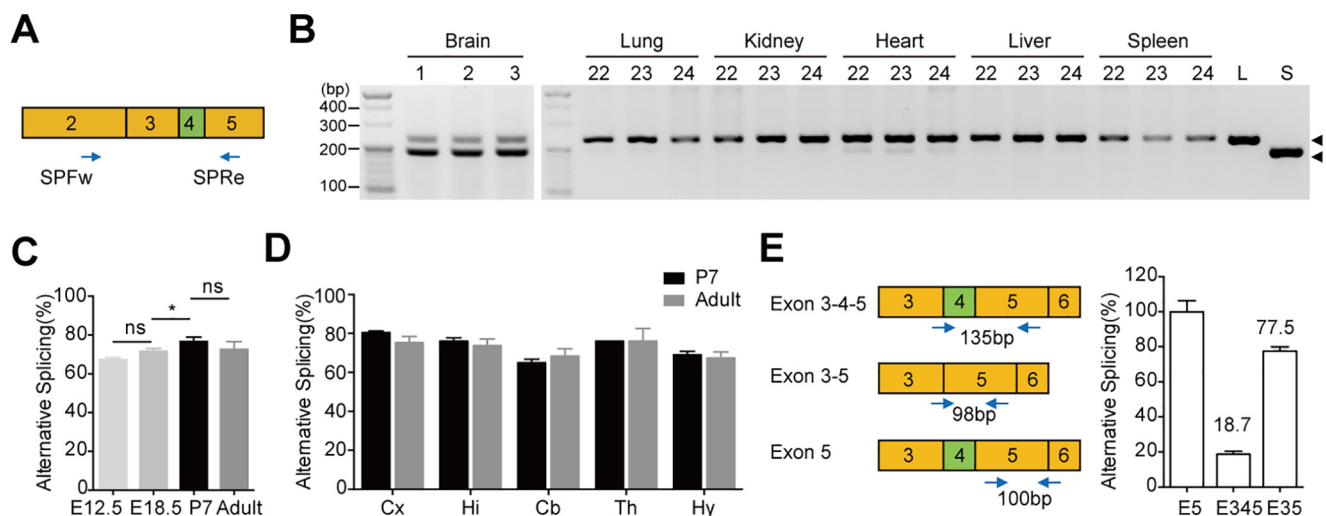


Figure 5. Alternative splicing of *Tmem63b* exon 4 in mouse brains. *A*, schematic representation of *Tmem63b* exons 3–5 in cDNA with exon 4 marked in green. SPFw and SPRre are primers for amplification. *B*, alternative splicing of *Tmem63b* exon 4 in brains, lungs, kidneys, hearts, livers, and spleens from three adult mice with codes labeled above. The amplified sequences with long and short forms were indicated by black arrowheads. *C*, quantification of alternative splicing levels in brains of E12.5 ($67.7 \pm 0.6\%$, $n = 3$), E18.5 ($72.0 \pm 1.0\%$, $n = 3$), P7 ($77.0 \pm 1.9\%$, $n = 5$), and adult ($73.0 \pm 3.6\%$, $n = 3$) mice. Data are shown as mean \pm S.D. (error bars) * $p < 0.05$; ns, not significant; one-way ANOVA, Tukey's post hoc test. *D*, quantification of alternative splicing levels in cerebral cortex (Cx), hippocampus (Hi), cerebellum (Cb), thalamus (Th), and hypothalamus (Hy) of P7 (black column) and adult (gray column) mice. Data are presented in Table S2 as mean \pm S.D. *E*, left, schematic representation of *Tmem63b* cDNA sequence from exon 3 to exon 6. Primers for amplification are indicated. Right, quantification of alternative splicing levels in brains of P7 mice by real-time PCR, which were similar to the results of agarose gel electrophoresis. E5, exon 5 ($n = 3$); E345, exon 3-4-5 without intron interval ($18.7 \pm 1.6\%$, $n = 3$); E35, exon 3-5 without intron interval ($77.5 \pm 2.6\%$, $n = 3$).

other (22–26). To test whether the Q/R editing at exon 20 and the splicing of exon 4 in *Tmem63b* pre-mRNA are also coupled, 40 *Tmem63b* clones originated from mouse brain were subjected to Sanger sequencing with full length, of which 36 were short cDNA clones lacking exon 4 and the majority of them (33/36) contained the edited R at the Q/R site. In contrast, all four long cDNA clones were not edited at the Q/R site (Fig. 6A). These data suggested that Q/R editing efficiency in long and short isoforms was biased. We further analyzed this phenotype using *Bsa*WI digestion. A pair of primers, with the forward primer base-paired to exon 4 (LFw) and the reverse one downstream of the Q/R site (CRe), was used to amplify the long isoform (2255 bp). The forward primer, with 4 bp of the 3' end base-paired to exon 5 and the rest of sequence base-paired to exon 3 (SFw), was designed to amplify the short isoform (2246 bp) (Fig. 6B). We found that the fragments amplified from short isoform were largely digested by *Bsa*WI (1593 bp and 653 bp) whereas the digestion bands were not seen in long-form *Tmem63b* fragments (Fig. 6, C and D). The Q/R editing was also limited to the short-form mRNAs of P7 and E18.5 mouse brains (Fig. S4, B and D), indicating that coupling is also present during development. As expected, the editing efficiency in short form was lower in young brains (Fig. 6E). The editing efficiency in short-form *Tmem63b* was further analyzed in different brain regions of P7 and adult mice. In adult, the editing was ~60% in hypothalamus and ~80% in other brain regions, whereas in P7, the editing in short-form mRNAs was generally lower in all brain regions as compared with those in adult (Fig. 6F and Fig. S4, A and C). To test whether Q/R editing is mutually excluded from the long-form *Tmem63b*, we subcloned the above fragments amplified from long- or short-form *Tmem63b* into pMD19-T vectors and subjected them to Sanger sequencing. In 44 clones of the long isoform, 42 contained unedited Q

and two clones were edited at the Q/R site. In contrast, 87% (13/15) of the clones amplified from the short isoform were edited to R at the Q/R site (Fig. 6G). Taken together, these results indicated that the alternative splicing of exon 4 and Q/R editing at exon 20 in *Tmem63b* pre-mRNA were coupled.

Presence of exon 4 suppresses Q/R editing in *Tmem63b*

We then studied which of the post-transcriptional modifications, the editing or the splicing, was dominant. We reasoned that if the editing determined the splicing efficiency as reported previously (22–24), then the alternative splicing of exon 4 would be absent in *Adar2* cKO mice. However, we found that the efficiency of alternative splicing was not changed (Fig. 7, A and B), suggesting that the editing did not affect the splicing.

To test the possibility that the splicing regulates the editing, we used primary culture of CGNs. We first examined the coupling of splicing and editing of endogenous *Tmem63b* in these neurons at DIV5, a time point at which we examined the transfected constructs (Fig. 7C). The splicing efficiency ($75.7 \pm 2.1\%$, $n = 3$, Fig. S5A) was close to that in the whole brain of P7 mice (Fig. 5C). The editing efficiency of endogenous *Tmem63b* in cultured CGNs was $28.7 \pm 2.1\%$ ($n = 3$, Fig. S5B), close to that in the P7 mouse cerebellum (~20%, Fig. 2D). Importantly, the editing was only detected in short isoforms using *Bsa*WI digestion, with editing efficiency of 37% (Fig. S5, C and D). We then examined the splicing and editing efficiencies of *Tmem63b* minigenes transfected in cultured CGNs. The editing segment of *Tmem63b* (Fig. 3A) was efficiently edited ($26.9 \pm 7.8\%$, $n = 7$) when transfected into CGNs (CTL, Fig. 7, D–F). The alternative splicing might modulate the editing through a *trans* mechanism, where the introns spliced out from long- or short-form *Tmem63b* regulate the editing, or a *cis* mechanism, where the mRNA sequence around the splicing region affects the editing.

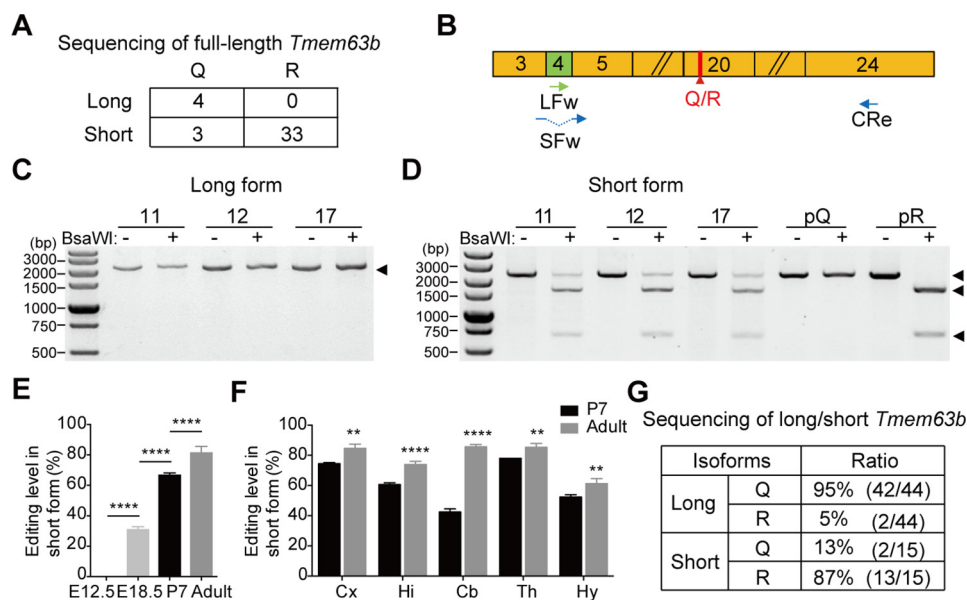


Figure 6. The coupling between exon 4 alternative splicing and Q/R editing in *Tmem63b* pre-mRNA. *A*, summary of the sequencing results of full-length *Tmem63b* cDNAs from mouse brain. *B*, schematic representation of *Tmem63b* exons 3–24 in cDNA. Primers for amplification are indicated. *C* and *D*, Q/R editing of long-form and short-form *Tmem63b* in brains from three adult mice with codons labeled above. The amplified sequences with long and short forms are indicated by black arrowheads. Plasmids with Q-form (pQ) and R-form (pR) *Tmem63b* cDNAs served as control to indicate the enzymatic activity of BsaWI. *E*, quantification of Q/R editing levels of short-form *Tmem63b* in brains of E12.5 (0.0 ± 0%, *n* = 3), E18.5 (31.3 ± 1.5%, *n* = 3), P7 (67.0 ± 1.2%, *n* = 5), and adult (81.7 ± 3.9%, *n* = 6) mice. Data are shown as mean ± S.D. (error bars). *****p* < 0.0001; one-way ANOVA, Tukey's post hoc test. *F*, quantification of Q/R editing levels of short-form *Tmem63b* in cerebral cortex (Cx), hippocampus (Hi), cerebellum (Cb), thalamus (Th), and hypothalamus (Hy) of P7 (black column) and adult (gray column) mice. Data are presented in Table S3 as mean ± S.D. ***p* < 0.01; *****p* < 0.0001; Student's *t* test, two-tailed. *G*, summary of the sequencing results of long-form and short-form *Tmem63b* from mouse brains.

For the long-form *Tmem63b*, the introns spliced out are intron 3 (I3) and intron 4 (I4), whereas in short form, the intronic segment spliced out is I3E4I4 (Fig. 7D). We found that all these intronic segments had no effects on the editing efficiency (Fig. 7, E and F), arguing against a *trans* mechanism. Then we constructed minigenes by fusing the editing segment with DNA segments containing exon 3~5 varied by alternative splicing of exon 4 (LiQi, LQi and SQi, Fig. 7G). The LiQi (genomic sequence from exon 3 to exon 5 linked with the editing segment) was largely (~65%) spliced to short form (Fig. 7I, lower panel). The editing efficiency in LiQi (17.4 ± 2.1%, *n* = 5) was close to SQi (exon 3-5 linked with the editing segment, 17.2 ± 3.3%, *n* = 5) but higher than LQi (exon 3-4-5 linked with the editing segment, 9.8 ± 3.8%, *n* = 5), indicating that the splicing regulates the editing in a *cis* manner. We then wondered whether the editing efficiency can be modified by changing splicing. We first made splicing site mutant (SpM), 5' splice site (GU) at intron 4 and 3' splice site (AG) at intron 3 mutated to complimentary nucleotides, which disrupts the inclusion of exon 4 (Fig. 7G). As expected, only the short-form transcript was observed. The editing in SpM (17.0 ± 2.4%, *n* = 5) was the same as SQi (Fig. 7, H and I). In neurons, multiple splicing factors such as Nova (34), Rbfox (35), nSR100 (36), Ptbp1, and Ptbp2 (37) enhance or silence splicing events through binding to specific RNA motifs. There are Nova binding motifs (YCA Y clusters) upstream of exon 4 (Fig. 7G) which could be involved in Nova-mediated exon skipping (38). These sites were then simultaneously mutated to obtain Nova binding motif mutant (NvM) (Fig. 7G). As expected, LiQi harboring these mutations significantly reduced the short isoform (~40% in NvM versus

~65% in WT LiQi). The editing efficiency was lower in NvM (12.4 ± 2.6%, *n* = 5) as compared with WT LiQi (Fig. 7, H and I). Taken together, these data indicate that the splicing of exon 4 regulated Q/R editing through a *cis* mechanism.

The Q/R editing affects Ca²⁺ permeability of *Tmem63b* channel

Tmem63 family are osmosensitive (or mechanosensitive) cation channels (27, 39). Their plant orthologue OSCA channels are also osmosensitive and mechanosensitive (39–41). The Cryo-EM structures of OSCA1.1 and OSCA1.2 have revealed protein domains that are responsible for differential channel properties, including mechanosensation, gating, ion selectivity, and dimer formation (40, 42, 43). To understand whether the editing and splicing affect the channel functions, we made a homology structural model for *Tmem63b* based on the cryo-EM structure of OSCA1.2 (Fig. 8, A–C) (42). The *Tmem63b* Q/R site is located at the intracellular mouth of the channel pore consisting of transmembrane helices M3–M7 (Fig. 8, A and B). A charged arginine residue at this position might interfere with the conductance of polyvalent cations, such as Ca²⁺. To test this possibility, we examined the Ca²⁺ conductance relative to Na⁺ for these four isoforms of *Tmem63b* in Neuro2a (N2a) cells (27). *Tmem63b*-mediated currents were recorded using a ramp protocol in whole-cell configuration by switching extracellular solution from 300 mOsm/liter to 170 mOsm/liter (Fig. 8, D and E). We recorded the currents using Na-gluconate in both extracellular and pipette solutions; gluconate was used to avoid the contamination from the endogenous Cl[−] currents (27). The osmolarity was adjusted by addition of mannitol

A splicing regulates a remote editing in *Tmem63b*

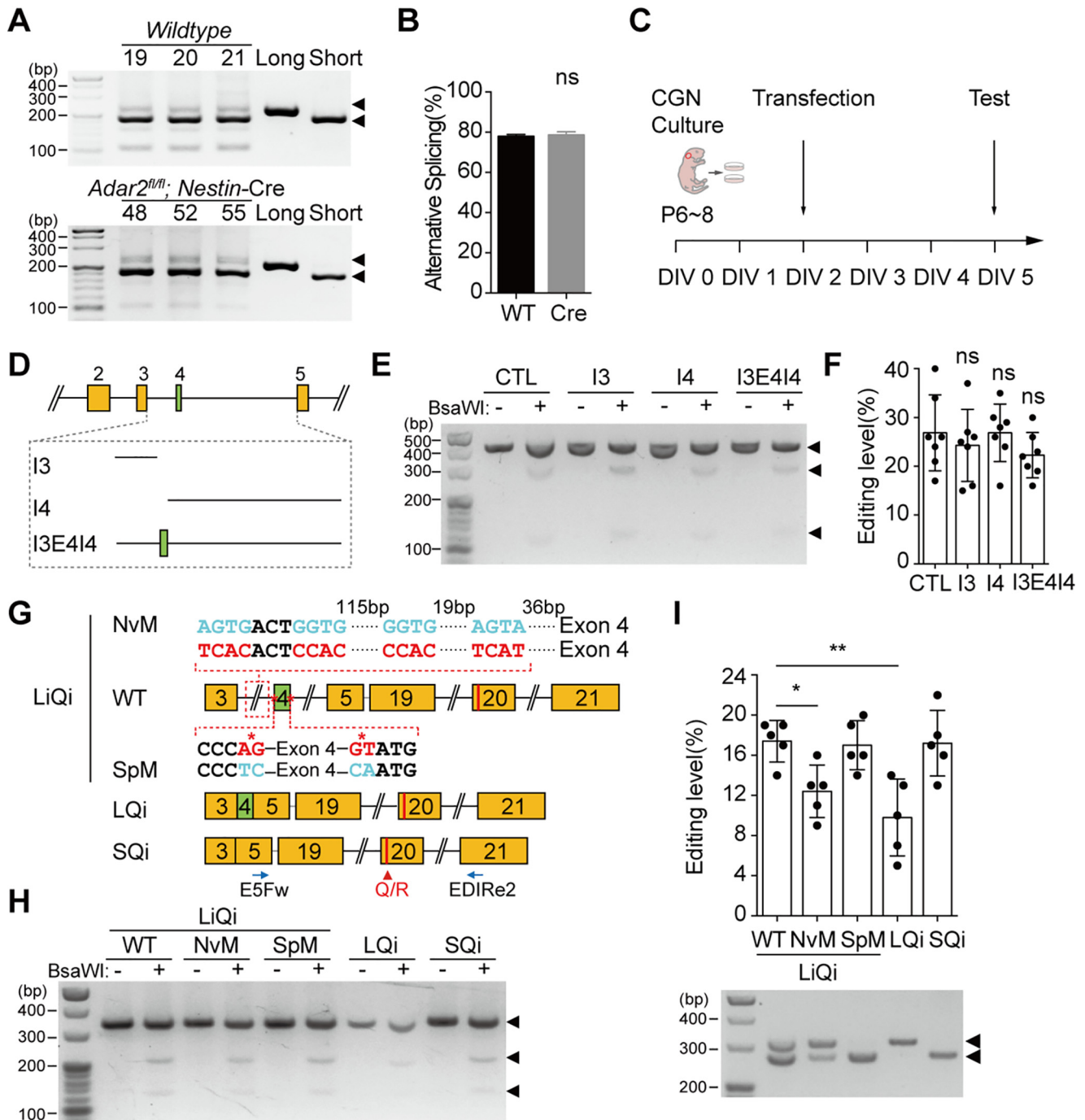


Figure 7. Alternative splicing of exon 4 regulates Q/R editing at exon 20. *A*, alternative splicing of exon 4 in brains of WT and *Adar2* cKO mice. *B*, quantification of alternative splicing levels in brains of WT ($78.0 \pm 1.0\%$, $n = 3$) and *Adar2* cKO ($78.7 \pm 1.5\%$, $n = 3$) mice. Data are shown as mean \pm S.D. *ns*, not significant; Student's *t* test, two-tailed. *C*, schematic demonstration of the experiments conducted in CGNs. *D*, schematic demonstration of the intronic segments spliced out in alternative splicing. *E* and *F*, Q/R editing efficiencies of the editing segment when cotransfected with I3 ($24.3 \pm 7.4\%$, $n = 7$), I4 ($26.9 \pm 5.9\%$, $n = 7$), I3E4I4 ($22.3 \pm 4.6\%$, $n = 7$), and vehicle control (CTL) ($26.9 \pm 7.8\%$, $n = 7$) in CGNs. Data are shown as mean \pm S.D. (error bars). *ns*, not significant; one-way ANOVA, Tukey's post hoc test. *G*, schematic demonstration of WT and mutant minigene constructs fusing the editing segment and splicing segment. E5Fw and EDIRE2 are primers for amplification. *H* and *I*, Q/R editing of fusion minigenes in CGNs. The Q/R editing efficiency was not changed in SQi ($17.2 \pm 3.3\%$, $n = 5$) and SpM ($17.0 \pm 2.4\%$, $n = 5$) but was suppressed in LQi ($9.8 \pm 3.8\%$, $n = 5$) and NvM ($12.4 \pm 2.6\%$, $n = 5$) mutant, compared with the LiQi control ($17.4 \pm 2.1\%$, $n = 5$). Lower panel in (*H*) shows the splicing levels corresponding to the upper editing event. Data are shown as mean \pm S.D. (error bars). * $p < 0.05$; ** $p < 0.01$; one-way ANOVA, Tukey's post hoc test.

without changing the ionic concentrations. After *Tmem63b* currents were induced by 170 mOsm/liter Na^+ solution and reached the amplitudes of ~ 600 pA (measured at -70 mV), the extracellular solution was switched to 170 mOsm/liter

Ca^{2+} solution. Because most reacting cells burst with continuous exposure to hypotonic solution, we did not try to record the currents at plateau in this experiment (27). The reversal potential in Na^+ solution was constant for all four isoforms,

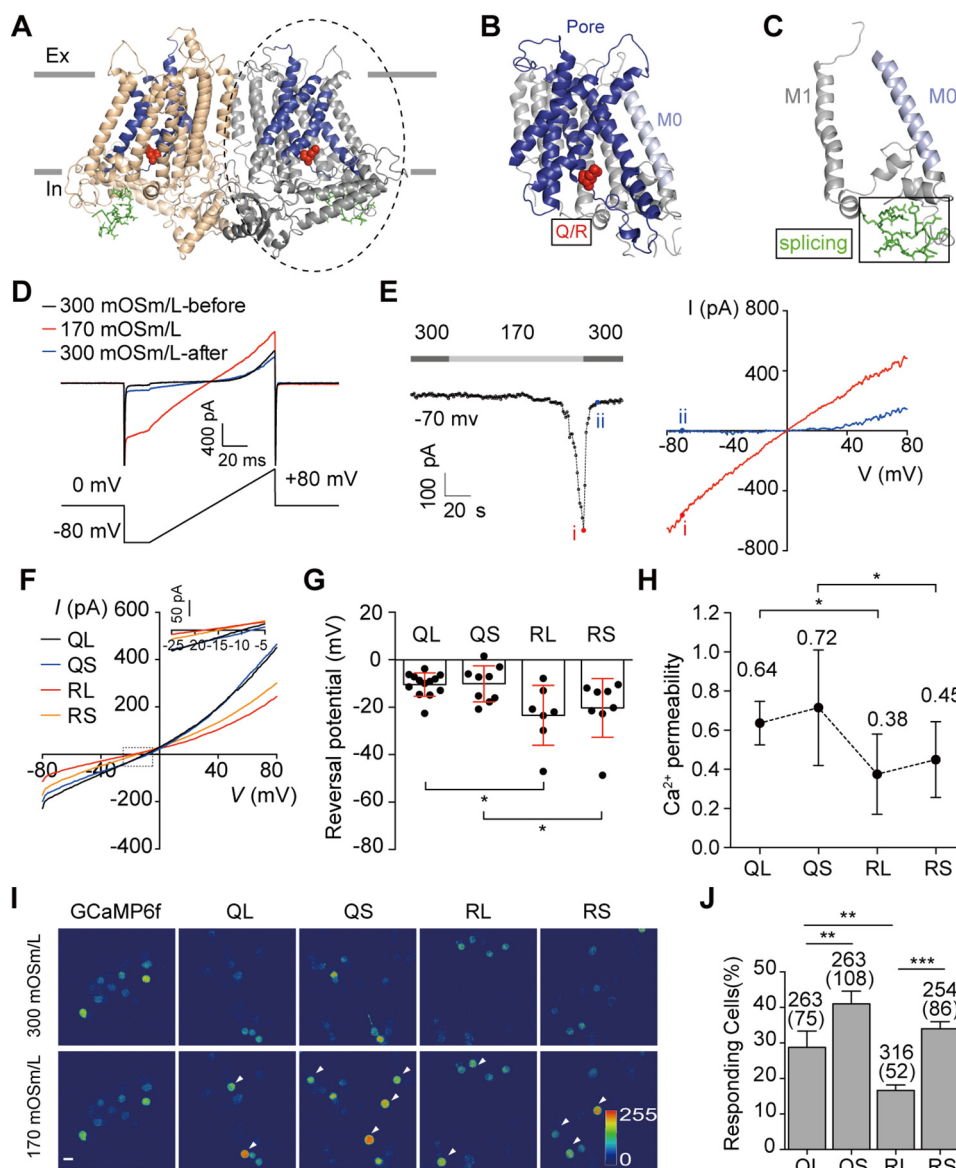


Figure 8. The splicing and the editing in *Tmem63b* regulate Ca^{2+} influx in response to hypotonic stimuli. A–C, the 3-dimensional homology model of mouse *Tmem63b* based on AtOSCA1.2 (PDB ID: 6mjv). The Q/R site (red sphere) is located at the intracellular mouth of channel pore (M3–M7, blue) (B). The exon 4 encoded amino acid in the first intracellular loop (green sticks) (C, D), the raw recording traces of *Tmem63b* (QL) currents responded to hypotonic stimuli. The cells were holding at 0 mV and recorded in whole-cell configuration by ramp protocol from -80 mV to 80 mV, 100-ms duration, 1 Hz. E, left, hypotonic solution gradually induced *Tmem63b* (QL) currents (measured at -70 mV). Right, I–V curves at the indicated time during hypotonic (red) to isotonic (blue) solutions. F, the averaged I–V curves after replacing Na^+ to Ca^{2+} in hypotonic perfusion solution. G, the reversal potential of Ca^{2+} measured by zero-current on I–V plots. QL (-10.4 ± 4.9 , $n = 13$), QS (-10.1 ± 7.6 , $n = 9$), RL (-23.4 ± 12.6 , $n = 7$), RS (-20.3 ± 12.4 , $n = 8$). Data are shown as mean \pm S.D. (error bars). * $p < 0.05$; one-way ANOVA, Tukey's post hoc test. H, the Ca^{2+} permeability relative to Na^+ ($P_{\text{Ca}}/P_{\text{Na}}$) was QL (0.64) \sim QS (0.72) $>$ RL (0.38) \sim RS (0.45). Data are shown as mean \pm S.D. (error bars). * $p < 0.05$; one-way ANOVA, Tukey's post hoc test. I, fluorescent emission images of N2a cells transfected with four *Tmem63b* isoforms, accompanied with the calcium-sensitive reporter GCaMP6f, in response to 170 mOsm/liter hypotonic stimuli. QL, the long isoform without editing, QS, the short isoform without editing. RL, the long isoform with the edited R. RS, the short isoform with the edited R. White arrowhead marks the responding cells. Scale bar, 10 μm . J, percentage of cells responding to 170 mOsm/liter hypotonic solutions. Numbers of cells tested and responding (in parentheses) are indicated above the bars. QL (28.8 \pm 4.6%, $n = 4$), QS (41.0 \pm 3.6%, $n = 3$), RL (16.7 \pm 1.5%, $n = 3$), RS (34.0 \pm 2.0%, $n = 3$). Data are shown as mean \pm S.D. ** $p < 0.01$; *** $p < 0.001$; ns, not significant; one-way ANOVA, Tukey's post hoc test.

-2.1 ± 2.1 mV for QL (the long isoform without editing, $n = 15$), -2.8 ± 2.8 mV for QS (the short isoform without editing, $n = 9$), -2.7 ± 2.2 mV for RL (the long isoform with the edited R, $n = 7$), and -2.9 ± 1.7 mV for RS (the short isoform with the edited R, $n = 8$). The reversal potential in Ca^{2+} solution was -10.4 ± 4.9 mV for QL ($n = 13$), -10.1 ± 7.6 mV for QS ($n = 9$), -23.4 ± 12.6 mV for RL ($n = 7$), and -20.3 ± 12.4 mV for RS ($n = 8$) (Fig. 8, F and G). The calculated Ca^{2+} permeability relative to Na^+ ($P_{\text{Ca}}/P_{\text{Na}}$) was QL (0.64) \sim QS (0.72) $>$

RL (0.38) \sim RS (0.45) (Fig. 8H). These data thus demonstrated that Q/R editing at the intracellular mouth of *Tmem63b* channel reduces Ca^{2+} permeability.

The splicing and editing regulate hypoosmolarity-induced Ca^{2+} influx

The exon 4 of *Tmem63b* encoded amino acids in the first intracellular loop 1 between M0 and M1 (Fig. 8, A and C). In *AtOSCA1.2*, the intracellular segment intracellular loop 2

A splicing regulates a remote editing in *Tmem63b*

paralleling plasma membrane is predicted to be involved in mechanosensation (42, 43). We recently demonstrated that *Tmem63s* are osmosensitive cation channels activated by hypotonic stress and mediate extracellular Ca^{2+} influx (27). We have established that the most sensitive measurement for the osmosensitivity was the percentage of cells responding to hypotonic stress (27). Interestingly, our measure of osmosensitivity is correlated with the whole-cell currents induced by negative pressure, a direct measure of mechanosensitivity in *Tmem63* family proteins (39), indicating that the osmosensitivity reflects the mechanosensitivity. Therefore, we examined the osmosensitivity of the four isoforms of *Tmem63b* using this established method. In brief, we expressed *Tmem63b* isoforms accompanied with the calcium reporter GCaMP6f (*Tmem63b*-P2A-GCaMP6f) in N2a cells (27). GCaMP6f fluorescence was monitored after switching the extracellular osmolarity from 300 mOsm/liter to 170 mOsm/liter. The $[\text{Ca}^{2+}]_i$ elevation was detected in cells expressing *Tmem63b* (Fig. 8J), but the ratios of responsive cells varied among four isoforms (Fig. 8J). Control cells that do not express *Tmem63b* failed to respond to hypotonic stimuli (Fig. 8J; 1/199). Hypoosmolarity-induced Ca^{2+} influx occurred more frequently in cells expressing the short form of *Tmem63b* (41% of QS and 34% of RS transfected cells) than in cells expressing the long forms (29% of QL and 17% of RL), indicating that exclusion of exon 4 enhanced the osmosensitivity of *Tmem63b* channel (Fig. 8J). These data also showed that Q-form *Tmem63b*s appeared to be more sensitive to osmolarity change than R-forms. Thus, the alternative splicing of exon 4 and the Q/R editing in *Tmem63b* coordinately regulate Ca^{2+} influx induced by hypoosmolarity.

Discussion

In this study, we have identified a coupling between the A-to-I editing at the Q/R site of exon 20 and the alternative splicing of exon 4 in *Tmem63b* pre-mRNAs in the mouse brain. Our study reveals that it displays the following properties. First, the occurrence sites for above post-transcriptional modifications are remote. Second, the alternative RNA splicing plays a dominant role.

In our observation, about 60% of *Tmem63b* mRNAs are edited at the Q/R site in the adult mouse brain, consistent with a previous study (44). The finding that this RNA editing event is brain-specific is also consistent with those reported recently (1, 45, 46). Furthermore, we demonstrate that the editing efficiencies vary in different brain regions at distinct development stages. Lastly, we show that the editing relies on Adar2, in line with previous observations (1, 46), and that the ECS is localized at the proximal 5' end of intron 20.

We have identified an alternative splicing of exon 4 in brain-originated *Tmem63b* mRNAs. The short *Tmem63b* mRNA isoform lacking exon 4 is the major form in the brain and accounts for about 80% of the total *Tmem63b* mRNAs. The splicing efficiency is constant in different brain regions and relatively stable at development stages. Like the editing, the alternative splicing also occurs mainly in the brain. Although the short isoform accounts for 2% of the total *Tmem63b* mRNAs in the heart, it is not observed in other tissues.

The Q/R editing and alternative splicing events in *Tmem63b* are coupled, in which the alternative splicing of exon 4 plays a dominant role. It has been shown that the exonic A-to-I editing and the splicing of nearby downstream introns often affect each other (22–26). This could well be explained by interference between the editing machinery and the spliceosomes that may simultaneously act on the adjacent loci on the pre-mRNA. To our knowledge, the interplay between an A-to-I editing and a distant alternative splicing has not been reported before. Our mechanistic analysis reveals that the Q/R editing of *Tmem63b* requires Adar2 binding to the hairpin structure formed by ECS and the editing region. Genetic deletion of Adar2 abolishes the Q/R editing, and mutations on the ECS impair the editing activity (Fig. 3, C–E and Fig. 4). We suspect that the splicing of exon 4 may regulate the stability of hairpin structure around the editing region or affect Adar2 capability in binding to the structure. Recent evidence has shown that Pin1 promotes the activity of Adar2 and increases the editing efficiencies (47). WWP2 and AIPM2 regulate the degradation of Adar2 to affect RNA editing (1, 47). The splicing factor SRSF9 downregulates Adar2-mediated RNA editing (46, 48). Interestingly, SRSF9 inhibits the *Tmem63b* Q/R editing in the mouse brain (46). Thus, it is possible that the splicing of exon 4 regulates the Q/R editing through some of the above factors.

We have demonstrated that the exon 4 alternative splicing and the Q/R editing regulate the osmosensitivity of *Tmem63b*. The Q/R site is located at the inner mouth of the *Tmem63b* channel pore (Fig. 8, A and B). A positively charged residue at this site reduces the permeability of divalent cation Ca^{2+} (Fig. 8H). A similar situation happens in α -amino-3-hydroxy-5-methyl-4-isoxazolepropionic acid receptor GluA2 and kainate receptors GluK1 and GluK2, where the Q/R editing occurs at the center of the channel pore and dictates the Ca^{2+} permeability (4, 49). The splicing site is located in intracellular loop 1 (Fig. 8, A and C). The structure studies on OSCA channels suggest that the α -helices in intracellular loop 2 paralleling membrane may involve mechanodetection and channel gating (42, 43). Our data demonstrated that the short-form *Tmem63s* are more sensitive to osmotic changes than long forms. The inclusion of exon 4 may interfere with the α -helices in intracellular loop 2 to change the mechanosensitivity of the channel or regulate osmosensitivity through undetermined mechanisms. It is very likely that the overall Ca^{2+} influx is determined by the Ca^{2+} permeability of the Q/R site combined with the mechanosensitivity of splicing sequences; thus, the apparent osmosensitivity reading by Ca^{2+} influx is QS > QL ~ RS > RL. Future studies are required to dissect physiological functions of *Tmem63b* isoforms in the brain.

Experimental procedures

Mice

All animal studies were approved by the Institutional Animal Care and Use Committee of Model Animal Research Center of Nanjing University and performed in accordance with guidelines for humane treatment of animals. All animals were housed in 12 h of light and 12 h of dark cycles at $25 \pm 1^\circ\text{C}$, with water and food obtained *ad libitum*. The *Adar2*^{fl/+} mouse line with

loxP site flanked exons 6–8 was generated through the bacterial artificial chromosome homologous recombination in embryonic stem cells at GemPharmatech (Nanjing). The founder mice were backcrossed with C57BL/6J mice for over five generations followed by breeding with *Nestin-Cre* mice (31) to obtain the brain-specific *Adar2* knockout mice (*Adar2^{fl/fl}; Nestin-Cre*). Genotypes were determined by PCR with the following primers: 5'-AGTCATTCCTCCTAGCCTTTT-3' (forward) and 5'-TTATCACCTTGGCATCTTTG-3' (reverse) to confirm the presence of the *loxP* site, 5'-ATTTGCCTGCAT-TACCGGTC-3' (forward) and 5'-ATCAACGTTTTCTT-TTCGG-3' (reverse) for the presence of *Cre*.

Cloning of *Tmem63b*, *Adar1*, and *Adar2* from mouse brains

The full-length coding sequences of *Tmem63b* (NM_198167.3), *Adar1* (*Adar*, NM_019655.3), and *Adar2* (*Adarb1*, NM_001024837.2) were amplified from mouse brain cDNAs, using specific primers (Table S4), by PrimeSTAR[®] HS DNA Polymerase (Takara Bio, R01A) and subcloned into pCAGGS vectors by Ligation-Free Cloning Kit (abm, E001) (50). For measuring the cytoplasmic calcium concentration, the free calcium indicator GCaMP6f was fused to the C-terminal of *Tmem63b* through a P2A linker (*Tmem63b*-P2A-GCaMP6f), leading to the separate expression of *Tmem63b* and GCaMP6f (27).

Generation of minigene constructs

In the study of A-to-I editing enzyme, the editing segment of *Tmem63b* and the *Htr2c* minigene with 211 bp spanning exon 5 and intron 5 were obtained from mouse genomic DNAs by specific primers (Table S4). The nucleotide in the “B” editing site of *Htr2c* was mutated from the unedited A to the edited G. To explore the ECS, a series of mutations on the editing segment and ECS were obtained through overlapping PCR and corresponding primers (Table S4). In the study of the coupling between alternative splicing of exon 4 and A-to-I editing at the Q/R site, the splicing segments (exon 3~5) amplified from mouse genomic DNAs and brain cDNAs were fused to the editing segment (LiQi, LQi and SQi) by overlapping PCR and corresponding primers (Table S4). The mutations on SpMs and NvMs were made on the WT LiQi minigene. The intronic segments spliced out from long- or short-form *Tmem63b*, including I3, I4, and I3E4I4, were obtained from mouse genomic DNAs by specific primers (Table S4). These minigenes were subcloned into pCAGGS vectors by Ligation-Free Cloning Kit (abm, E001).

Cell culture and transfection

HEK 293 cells were cultured in DMEM with 10% FBS (Gibco). The minigenes were transfected into cells using lipofectamine 2000 according to the manufacturer's instruction. The cells were collected for analysis 24–48 h after transfection. CGNs were acutely dissected and cultured following the protocols reported in previous studies (51). In brief, CGNs were prepared from cerebellums of WT mice at P6-8 and plated at a density of 5×10^5 cells/cm² in 10-cm dishes. The cells were cultured in Basal Medium Eagle-based medium containing 10% FBS, 22 mM KCl, 2% B27, 2 mM L-glutamine, and 1% penicillin-

streptomycin (all from Gibco) for 2 days. At DIV 2, primary cultured neurons were transfected with *Tmem63b* minigenes using lipofectamine 2000, and the medium was replaced with MEM-based medium containing 5 mg/ml D-glucose (Sigma-Aldrich), 1% ITS (insulin-transferrin-sodium selenite) (Sigma-Aldrich), 2 mM L-glutamine, and 1% penicillin-streptomycin. CGNs were collected for analysis 48–72 h after transfection.

RNA isolation and quantitative real-time PCR

For cloning and quantification of mRNA isoforms of *Tmem63b* in tissues, total RNA samples from mouse tissues were extracted by TRIzol (Invitrogen) and reverse-transcribed into cDNAs using HiScript[®] 1st Strand cDNA Synthesis Kit (Vazyme Biotech, R111) and oligo(dT)18 primer. For cultured cells transfected with *Tmem63b* or *Htr2c* minigenes, the extracted total RNAs were digested by RNase-free DNaseI (Life Technologies, AM2238) at 37 °C for 1 h to remove the endogenous genomic and transfected DNAs. Then the RNAs were reverse-transcribed into cDNAs by specific reverse transcription primer, 5'-GAATGCTCGTCAAGAAGAC-3' (RT_{IR}ES), using HiScript[®] 1st Strand cDNA Synthesis Kit (Vazyme, R111). Only the RNAs from exogenous constructs could be reverse-transcribed. The RT (minus) controls of each experiment were carried out to assess the amount of DNA contaminations in RNA preparations.

For quantitative real-time PCR, the RNA samples from mouse brains were reverse-transcribed into cDNAs using HiScript Q RT SuperMix for qPCR (+gDNA wiper) Kit (Vazyme Biotech, R123). cDNAs of different *Tmem63b* isoforms were quantified by Applied Biosystems StepOnePlus Real-Time PCR system (Life Technologies) using AceQ[®] qPCR SYBR[®] Green Master (High ROX Premixed) (Vazyme Biotech, Q141) reagents with specific primer pairs: exon 3-4-5, 5'-ACAGATGCAGACAGGCTTC-3' and 5'-TTGGTCAAAGTCGACAGAGC-3'; exon 3-5, 5'-TGACAGATGCAGACAGTGTG-3' and 5'-TTGGTCAAAGTCGACAGAGC-3'; exon 5, 5'-ATCAGCTATGCATGGGGAC-3' and 5'-CCAGGAACAGAAAGCCATTG-3'; and *Gapdh*, 5'-TGAACGGGAAGCTCAC-TGG-3' and 5'-TCCACCACCCTGTTGCTGTA-3'.

Quantification of RNA editing

For quantification of Q/R editing in mouse tissues, the genomic sequences spanning the editing site (311 bp) were amplified by primers EDIFw1 (forward) and EDIRe1 (reverse). The cDNA sequences spanning the Q/R site (327 bp) were amplified by primers EDIFw2 (forward) and EDIRe2 (reverse). In the study of A-to-I editing enzyme and ECS in HEK293 cells, the cDNA sequences of transfected *Tmem63b* minigene (403 bp) were amplified by primers pCAGFw (forward) and EDIRe2 (reverse). The cDNA sequence of transfected *Htr2c* minigene (340 bp) was amplified by primers pCAGFw (forward) and pCAGRe (reverse). In the experiment to study the coupling between alternative splicing of exon 4 and Q/R editing at exon 20 in mouse brain cDNAs, the primers LFw (forward) and CRe (reverse) were designed to amplify the long-form (2255 bp) *Tmem63b*, whereas the short-form (2246 bp) *Tmem63b* fragments were amplified by SFw (forward) and CRe (reverse). In

A splicing regulates a remote editing in *Tmem63b*

the experiment to explore the regulation of splicing to editing in CGNs, the cDNA sequences of transfected *Tmem63b* minigene were amplified by following primers: pCAGFw and EDIRE2 for the study of *trans* regulation, resulting in the PCR a product of 403 bp; and E5Fw (forward) and EDIRE2 (reverse) for the study of *cis* regulation, resulting in the PCR a product of 334 bp. The primers used in above amplification were shown in Table S4.

For *Tmem63b*, the amplified fragments were incubated with BsaWI endonuclease at 60 °C for 1 h and resolved by agarose gel electrophoresis. For *Htr2c*, the amplified fragments were incubated with BtsI endonuclease at 55 °C for 1 h and resolved by agarose gel electrophoresis. The gels were scanned by Gel Imaging System (Tanon). The abundance of each band was analyzed by ImageJ software (National Institutes of Health). The efficiency of editing was displayed by the ratio of integrated densities of BsaWI enzymed bands to control bands. In analysis of ECS, because the BsaWI recognition site is disrupted when the mutations are nearby Q/R site, the editing efficiencies of these mutants were quantified by measuring the ratio of peak heights obtained from sequencing chromatograms.

Quantification of mRNA splicing isoforms

A pair of primers with forward (SPFw) and reverse (SPRe) were designed to amplify the cDNA sequence near the splicing region (Table S4). *Tmem63b* cDNAs with (long-form) or without (short-form) exon 4 were amplified into different lengths (223 bp and 184 bp), followed by agarose gel electrophoresis. The long (309 bp) and short (270 bp) isoforms from LiQi minigenes were amplified by pCAGFw (forward) and E5Re (reverse), followed by agarose gel electrophoresis (Table S4). The gels were scanned by Gel Imaging System (Tanon). The abundance of each band was analyzed by ImageJ software (National Institutes of Health). The values were normalized according to bands size difference. The efficiency of exon 4 alternative splicing was displayed by the ratio of integrated densities of short form bands to total.

Cytoplasmic Ca^{2+} measurements

The cytoplasmic calcium concentration was monitored by free calcium indicator GCaMP6f (27). *Tmem63b*-P2A-GCaMP6f vectors were transfected into N2a cells mounted on the coverslip. GCaMP6f vector was used as a control. 40 h after transfection, the cells were perfused with isotonic extracellular solution (in mM): 65 NaCl, 5 KCl, 1 CaCl₂, 1 MgCl₂, and 10 HEPES (pH 7.4 adjusted with NaOH; 300 mOsm/liter adjusted with mannitol). The isotonic solution was exchanged to 170 mOsm/liter hypotonic solution without changing the ionic concentrations by a peristaltic pump (BT100-2J, Longer Precision Pump Co., Ltd., Hebei, China) at a constant speed. The osmolarity was measured by a vapor pressure osmometer (Wescor Vapro Model 5600). The cytoplasmic calcium fluorescence was recorded at 1 Hz for 10 min by laser scanning confocal microscope (Leica Microsystems, TCS SP2) at room temperature (24 ± 2 °C) using 488-nm illumination. The change of fluorescence was normalized by the ratio of real-time intensity (Ft) relative to the

initial value (F0). The cells with Ft/F0 > 1.5 were considered as positive cells responding to osmolarity changes.

N2a cell electrophysiology

Whole-cell patch clamp recordings were performed on transfected N2a cells under ramp protocol. The recording electrodes had the resistance of 8~10 MΩ when filled with the pipette solution composed of (in mM) 80 Na-gluconate, 130 mannitol, and 10 HEPES (pH 7.4 with NaOH, 300 mOsm/liter). The cells were perfused with isotonic extracellular solution containing (in mM) 80 Na-gluconate, 1 Ca-gluconate, 10 HEPES, and 130 mannitol (pH 7.4 with NaOH, 300 mOsm/liter). The hypotonic extracellular solution without changing the ionic concentration contains (in mM) 80 Na-gluconate, 1 Ca-gluconate, and 10 HEPES (pH 7.4 with NaOH, 170 mOsm/liter). For measuring the Ca²⁺ permeability, the Na⁺-rich hypotonic extracellular solution was changed to Ca²⁺-rich solution containing (in mM) 40 Ca-gluconate, 40 mannitol, and 10 HEPES (pH 7.4 with Ca(OH)₂, 170 mOsm/liter). The currents were collected using an Axopatch 200B amplifier and Digidata 1550 digitizer (Molecular Devices) at the sampling rate of 10 kHz and were low-pass filtered at 1 kHz. The current data were analyzed using pClamp 10 software. The cells were holding at 0 mV before application of 100-ms ramp from -80 mV to 80 mV every 1 s. The cells with a membrane resistance below 800 MΩ or series resistance above 10 MΩ were discarded. The Ca²⁺ permeability relative to Na⁺ (P_{Ca}/P_{Na}) was calculated as $P_{Ca}/P_{Na} = [Na^+]_i \exp(\Delta V_{rev} F/RT) / (1 + \exp(\Delta V_{rev} F/RT)) / 4[Ca^{2+}]_o$, where the ΔV_{rev} is measured the shift in reversal potential, $[Na^+]_i$ is the intracellular Na⁺ concentration, and $[Ca^{2+}]_o$ is the concentration of the extracellular substituting Ca²⁺. The reversal potential was measured in 7–13 cells for each isoform.

RNA secondary structure prediction

The secondary structures of RNA around the editing site and the ECS were predicted by RNAstructure software (Version 6.0.1). The sequence 200 bases downstream and upstream of the editing site was imported for analysis. The lowest free energy structure and a set of low free energy structures were predicted according to following restrictions on parameters: Maximum % Energy Difference, Maximum Number of Structures, and Window Size. The parameters were set as previously reported (33). The Maximum % Energy Difference was 10%. The Maximum Number of Structures was 20. The Window Size was 3.

Homology modeling

Protein sequence of mouse *Tmem63b* was aligned to *AtOSCA1.2*, the plant homolog of *Tmem63b* with Cryo-EM structure solved (42, 43). The homology modeling of mouse *Tmem63b* was obtained using SWISS-MODEL server (53) with the template of *AtOSCA1.2* (PDB ID: 6mjv). The model was depicted by PyMol program.

Statistical analysis

All data are presented as mean ± standard deviation (S.D.) in at least three independent experiments. Statistical analyses

were performed using GraphPad Prism version 6.0c software and analyzed using one-way analysis of variance (ANOVA) or unpaired *t* test if not otherwise stated. *p* values less than 0.05 were considered statistically significant. **p* < 0.05; ***p* < 0.01; ****p* < 0.001; *****p* < 0.0001. *p* ≥ 0.05 was denoted as “*ns*.”

Data availability

All data supporting our conclusions are contained within this article and in the [supporting information](#).

Acknowledgments—We thank all members in Shi lab for helpful discussion.

Author contributions—D. W., Y.-Y. Z., Y.-Y. S., C. Y., W.-M. C., and X.-H. T. investigation; D. W. writing-original draft; L. Z., Y. L., Z. G., and G.-q. C. resources; Y. X., J.-J. Y., and Y. S. S. supervision; J.-J. Y. and Y. S. S. conceptualization; Y. S. S. funding acquisition; Y. S. S. writing-review and editing.

Funding and additional information—This work is supported by the National Key R&D Program of China Grant 2019YFA0801603 (to Y. S. S.), the National Natural Science Foundation of China Grants 91849112 and 31571060 (to Y. S. S.), the Natural Science Foundation of Jiangsu Province Grants BK20140018 and BE2019707 (to Y. S. S.), and the Fundamental Research Funds for the Central Universities Grant 0903-14380029 (to Y. S. S.).

Abbreviations—The abbreviations used are: Adar, adenosine deaminases acting on RNA; ECS, editing site complementary sequence; CGN, cerebellar granule neurons; I3, intron 3; I4, intron 4; E4, exon 4; SpM, splicing site motif; NvM, Nova binding motif; N2a, Neuro2a; ANOVA, analysis of variance.

References

- Tan, M. H., Li, Q., Shanmugam, R., Piskol, R., Kohler, J., Young, A. N., Liu, K. I., Zhang, R., Ramaswami, G., Ariyoshi, K., Gupte, A., Keegan, L. P., George, C. X., Ramu, A., Huang, N., *et al.* (2017) Dynamic landscape and regulation of RNA editing in mammals. *Nature* **550**, 249–254 [CrossRef Medline](#)
- Basilio, C., Wahba, A. J., Lengyel, P., Speyer, J. F., and Ochoa, S. (1962) Synthetic polynucleotides and the amino acid code. *V. Proc. Natl. Acad. Sci. U. S. A.* **48**, 613–616 [CrossRef Medline](#)
- Sommer, B., Köhler, M., Sprengel, R., and Seeburg, P. H. (1991) RNA editing in brain controls a determinant of ion flow in glutamate-gated channels. *Cell* **67**, 11–19 [CrossRef Medline](#)
- Köhler, M., Burnashev, N., Sakmann, B., and Seeburg, P. H. (1993) Determinants of Ca²⁺ permeability in both TM1 and TM2 of high affinity kainate receptor channels: diversity by RNA editing. *Neuron* **10**, 491–500 [CrossRef Medline](#)
- Hoopengardner, B., Bhalla, T., Staber, C., and Reenan, R. (2003) Nervous system targets of RNA editing identified by comparative genomics. *Science* **301**, 832–836 [CrossRef Medline](#)
- Burns, C. M., Chu, H., Rueter, S. M., Hutchinson, L. K., Canton, H., Sanders-Bush, E., and Emeson, R. B. (1997) Regulation of serotonin-2C receptor G-protein coupling by RNA editing. *Nature* **387**, 303–308 [CrossRef Medline](#)
- Behm, M., and Öhman, M. (2016) RNA editing: A contributor to neuronal dynamics in the mammalian brain. *Trends Genet.* **32**, 165–175 [CrossRef Medline](#)
- Liu, S. J., and Zukin, R. S. (2007) Ca²⁺-permeable AMPA receptors in synaptic plasticity and neuronal death. *Trends Neurosci.* **30**, 126–134 [CrossRef Medline](#)
- Whitney, N. P., Peng, H., Erdmann, N. B., Tian, C., Monaghan, D. T., and Zheng, J. C. (2008) Calcium-permeable AMPA receptors containing Q/R-unedited GluR2 direct human neural progenitor cell differentiation to neurons. *FASEB J.* **22**, 2888–2900 [CrossRef Medline](#)
- Peng, P. L., Zhong, X., Tu, W., Soundarapandian, M. M., Molner, P., Zhu, D., Lau, L., Liu, S., Liu, F., and Lu, Y. (2006) ADAR2-dependent RNA editing of AMPA receptor subunit GluR2 determines vulnerability of neurons in forebrain ischemia. *Neuron* **49**, 719–733 [CrossRef Medline](#)
- Higuchi, M., Single, F. N., Köhler, M., Sommer, B., Sprengel, R., and Seeburg, P. H. (1993) RNA editing of AMPA receptor subunit GluR-B: a base-paired intron-exon structure determines position and efficiency. *Cell* **75**, 1361–1370 [CrossRef Medline](#)
- Nilsen, T. W., and Graveley, B. R. (2010) Expansion of the eukaryotic proteome by alternative splicing. *Nature* **463**, 457–463 [CrossRef Medline](#)
- Pan, Q., Shai, O., Lee, L. J., Frey, B. J., and Blencowe, B. J. (2008) Deep surveying of alternative splicing complexity in the human transcriptome by high-throughput sequencing. *Nat. Genet.* **40**, 1413–1415 [CrossRef Medline](#)
- Wang, E. T., Sandberg, R., Luo, S., Khrebukova, I., Zhang, L., Mayr, C., Kingsmore, S. F., Schroth, G. P., and Burge, C. B. (2008) Alternative isoform regulation in human tissue transcriptomes. *Nature* **456**, 470–476 [CrossRef Medline](#)
- Treisman, R., Orkin, S. H., and Maniatis, T. (1983) Specific transcription and RNA splicing defects in five cloned β -thalassaemia genes. *Nature* **302**, 591–596 [CrossRef Medline](#)
- Rockenstein, E. M., McConlogue, L., Tan, H., Power, M., Masliah, E., and Mucke, L. (1995) Levels and alternative splicing of amyloid beta protein precursor (APP) transcripts in brains of APP transgenic mice and humans with Alzheimer's disease. *J. Biol. Chem.* **270**, 28257–28267 [CrossRef Medline](#)
- Raj, T., Li, Y. I., Wong, G., Humphrey, J., Wang, M., Ramdhani, S., Wang, Y. C., Ng, B., Gupta, I., Haroutunian, V., Schadt, E. E., Young-Pearse, T., Mostafavi, S., Zhang, B., Sklar, P., *et al.* (2018) Integrative transcriptome analyses of the aging brain implicate altered splicing in Alzheimer's disease susceptibility. *Nat. Genet.* **50**, 1584–1592 [CrossRef Medline](#)
- Kashima, T., and Manley, J. L. (2003) A negative element in SMN2 exon 7 inhibits splicing in spinal muscular atrophy. *Nat. Genet.* **34**, 460–463 [CrossRef Medline](#)
- Kim, H. J., Kim, N. C., Wang, Y. D., Scarborough, E. A., Moore, J., Diaz, Z., MacLea, K. S., Freibaum, B., Li, S., Molliex, A., Kanagaraj, A. P., Carter, R., Boylan, K. B., Wojtas, A. M., Rademakers, R., *et al.* (2013) Mutations in prion-like domains in hnRNPA2B1 and hnRNPA1 cause multisystem proteinopathy and ALS. *Nature* **495**, 467–473 [CrossRef Medline](#)
- Perrone, B., La Cognata, V., Sprovieri, T., Ungaro, C., Conforti, F. L., Andò, S., and Cavallaro, S. (2020) Alternative splicing of ALS genes: Misregulation and potential therapies. *Cell. Mol. Neurobiol.* **40**, 1–14 [CrossRef Medline](#)
- Song, X., Zeng, Z., Wei, H., and Wang, Z. (2018) Alternative splicing in cancers: From aberrant regulation to new therapeutics. *Semin. Cell Dev. Biol.* **75**, 13–22 [CrossRef Medline](#)
- Penn, A. C., Balik, A., and Greger, I. H. (2013) Steric antisense inhibition of AMPA receptor Q/R editing reveals tight coupling to intronic editing sites and splicing. *Nucleic Acids Res.* **41**, 1113–1123 [CrossRef Medline](#)
- Schoft, V. K., Schopoff, S., and Jantsch, M. F. (2007) Regulation of glutamate receptor B pre-mRNA splicing by RNA editing. *Nucleic Acids Res.* **35**, 3723–3732 [CrossRef Medline](#)
- Bratt, E., and Öhman, M. (2003) Coordination of editing and splicing of glutamate receptor pre-mRNA. *RNA* **9**, 309–318 [CrossRef Medline](#)
- Licht, K., Kapoor, U., Mayrhofer, E., and Jantsch, M. F. (2016) Adenosine to inosine editing frequency controlled by splicing efficiency. *Nucleic Acids Res.* **44**, 6398–6408 [CrossRef Medline](#)
- Licht, K., Kapoor, U., Amman, F., Picardi, E., Martin, D., Bajad, P., and Jantsch, M. F. (2019) A high resolution A-to-I editing map in the mouse identifies editing events controlled by pre-mRNA splicing. *Genome Res.* **29**, 1453–1463 [CrossRef Medline](#)

A splicing regulates a remote editing in *Tmem63b*

27. Du, H., Ye, C., Wu, D., Zang, Y. Y., Zhang, L., Chen, C., He, X. Y., Yang, J. J., Hu, P., Xu, Z., Wan, G., and Shi, Y. S. (2020) The cation channel TMEM63B is an osmosensor required for hearing. *Cell Rep.* **31**, 107596 [CrossRef Medline](#)
28. Schulz, A., Müller, N. V., van de Lest, N. A., Eisenreich, A., Schmidbauer, M., Barysenka, A., Purfürst, B., Sporbart, A., Lorenzen, T., Meyer, A. M., Herlan, L., Witten, A., Ruhle, F., Zhou, W., de Heer, E., *et al.* (2019) Analysis of the genomic architecture of a complex trait locus in hypertensive rat models links *Tmem63c* to kidney damage. *eLife* **8**, e42068 [CrossRef Medline](#)
29. Yan, H., Helman, G., Murthy, S. E., Ji, H., Crawford, J., Kubisiak, T., Bent, S. J., Xiao, J., Taft, R. J., Coombs, A., Wu, Y., Pop, A., Li, D., de Vries, L. S., Jiang, Y., *et al.* (2019) Heterozygous variants in the mechanosensitive ion channel TMEM63A result in transient hypomyelination during infancy. *Am. J. Hum. Genet.* **105**, 996–1004 [CrossRef Medline](#)
30. Fukuda, M., Oyama, Y., Nishitarumizu, A., Omura, M., Nose, K., and Deshimaru, M. (2015) Identification of an RNA element for specific coordination of A-to-I RNA editing on HTR2C pre-mRNA. *Genes Cells* **20**, 834–846 [CrossRef Medline](#)
31. Tronche, F., Kellendonk, C., Kretz, O., Gass, P., Anlag, K., Orban, P. C., Bock, R., Klein, R., and Schütz, G. (1999) Disruption of the glucocorticoid receptor gene in the nervous system results in reduced anxiety. *Nat. Genet.* **23**, 99–103 [CrossRef Medline](#)
32. Higuchi, M., Maas, S., Single, F. N., Hartner, J., Rozov, A., Burnashev, N., Feldmeyer, D., Sprengel, R., and Seeburg, P. H. (2000) Point mutation in an AMPA receptor gene rescues lethality in mice deficient in the RNA-editing enzyme ADAR2. *Nature* **406**, 78–81 [CrossRef Medline](#)
33. Reuter, J. S., and Mathews, D. H. (2010) RNAstructure: software for RNA secondary structure prediction and analysis. *BMC Bioinformatics* **11**, 129 [CrossRef Medline](#)
34. Ule, J., Ule, A., Spencer, J., Williams, A., Hu, J. S., Cline, M., Wang, H., Clark, T., Fraser, C., Ruggiu, M., Zeeberg, B. R., Kane, D., Weinstein, J. N., Blume, J., and Darnell, R. B. (2005) Nova regulates brain-specific splicing to shape the synapse. *Nat. Genet.* **37**, 844–852 [CrossRef Medline](#)
35. Lovci, M. T., Ghanem, D., Marr, H., Arnold, J., Gee, S., Parra, M., Liang, T. Y., Stark, T. J., Gehman, L. T., Hoon, S., Massirer, K. B., Pratt, G. A., Black, D. L., Gray, J. W., Conboy, J. G., *et al.* (2013) Rbfox proteins regulate alternative mRNA splicing through evolutionarily conserved RNA bridges. *Nat. Struct. Mol. Biol.* **20**, 1434–1442 [CrossRef Medline](#)
36. Calarco, J. A., Superina, S., O'Hanlon, D., Gabut, M., Raj, B., Pan, Q., Skalska, U., Clarke, L., Gelinis, D., van der Kooy, D., Zhen, M., Ciruna, B., and Blencowe, B. J. (2009) Regulation of vertebrate nervous system alternative splicing and development by an SR-related protein. *Cell* **138**, 898–910 [CrossRef Medline](#)
37. Boutz, P. L., Stoilov, P., Li, Q., Lin, C. H., Chawla, G., Ostrow, K., Shiue, L., Ares, M., and Black, D. L. (2007) A post-transcriptional regulatory switch in polypyrimidine tract-binding proteins reprograms alternative splicing in developing neurons. *Genes Dev.* **21**, 1636–1652 [CrossRef Medline](#)
38. Ule, J., Stefani, G., Mele, A., Ruggiu, M., Wang, X., Taneri, B., Gaasterland, T., Blencowe, B. J., and Darnell, R. B. (2006) An RNA map predicting Nova-dependent splicing regulation. *Nature* **444**, 580–586 [CrossRef Medline](#)
39. Murthy, S. E., Dubin, A. E., Whitwam, T., Jojoa-Cruz, S., Cahalan, S. M., Mousavi, S. A. R., Ward, A. B., and Patapoutian, A. (2018) OSCA/TMEM63 are an evolutionarily conserved family of mechanically activated ion channels. *eLife* **7**, [CrossRef Medline](#)
40. Zhang, M., Wang, D., Kang, Y., Wu, J. X., Yao, F., Pan, C., Yan, Z., Song, C., and Chen, L. (2018) Structure of the mechanosensitive OSCA channels. *Nat. Struct. Mol. Biol.* **25**, 850–858 [CrossRef Medline](#)
41. Yuan, F., Yang, H., Xue, Y., Kong, D., Ye, R., Li, C., Zhang, J., Theprungsirikul, L., Shrift, T., Krichilsky, B., Johnson, D. M., Swift, G. B., He, Y., Siedow, J. N., and Pei, Z. M. (2014) OSCA1 mediates osmotic-stress-evoked Ca²⁺ increases vital for osmosensing in Arabidopsis. *Nature* **514**, 367–371 [CrossRef Medline](#)
42. Jojoa-Cruz, S., Saotome, K., Murthy, S. E., Tsui, C. C. A., Sansom, M. S., Patapoutian, A., and Ward, A. B. (2018) Cryo-EM structure of the mechanically activated ion channel OSCA1.2. *eLife* **7**, e41845 [CrossRef Medline](#)
43. Liu, X., Wang, J., and Sun, L. (2018) Structure of the hyperosmolality-gated calcium-permeable channel OSCA1.2. *Nat. Commun.* **9**, 5060 [CrossRef Medline](#)
44. Danecek, P., Nellåker, C., McIntyre, R. E., Buendia-Buendia, J. E., Bumpstead, S., Ponting, C. P., Flint, J., Durbin, R., Keane, T. M., and Adams, D. J. (2012) High levels of RNA-editing site conservation amongst 15 laboratory mouse strains. *Genome Biol.* **13**, 26 [CrossRef Medline](#)
45. Gal-Mark, N., Shallev, L., Sweetat, S., Barak, M., Billy Li, J., Levanon, E. Y., Eisenberg, E., and Behar, O. (2017) Abnormalities in A-to-I RNA editing patterns in CNS injuries correlate with dynamic changes in cell type composition. *Sci. Rep.* **7**, 43421 [CrossRef Medline](#)
46. Shanmugam, R., Zhang, F., Srinivasan, H., Charles Richard, J. L., Liu, K. I., Zhang, X., Woo, C. W. A., Chua, Z. H. M., Buschdorf, J. P., Meaney, M. J., and Tan, M. H. (2018) SRSF9 selectively represses ADAR2-mediated editing of brain-specific sites in primates. *Nucleic Acids Res.* **46**, 7379–7395 [CrossRef Medline](#)
47. Marcucci, R., Brindle, J., Paro, S., Casadio, A., Hempel, S., Morrice, N., Bisso, A., Keegan, L. P., Del Sal, G., and O'Connell, M. A. (2011) Pin1 and WWP2 regulate GluR2 Q/R site RNA editing by ADAR2 with opposing effects. *EMBO J.* **30**, 4211–4222 [CrossRef Medline](#)
48. Huang, H., Kapeli, K., Jin, W., Wong, Y. P., Arumugam, T. V., Koh, J. H., Srimasorn, S., Mallilankaraman, K., Chua, J. J. E., Yeo, G. W., and Soong, T. W. (2018) Tissue-selective restriction of RNA editing of CaV1.3 by splicing factor SRSF9. *Nucleic Acids Res.* **46**, 7323–7338 [CrossRef Medline](#)
49. Burnashev, N., Monyer, H., Seeburg, P. H., and Sakmann, B. (1992) Divalent ion permeability of ampa receptor channels is dominated by the edited form of a single subunit. *Neuron* **8**, 189–198 [CrossRef Medline](#)
50. Duan, G. F., Ye, Y., Xu, S., Tao, W., Zhao, S., Jin, T., Nicoll, R. A., Shi, Y. S., and Sheng, N. (2018) Signal peptide represses GluK1 surface and synaptic trafficking through binding to amino-terminal domain. *Nat. Commun.* **9**, 4879 [CrossRef Medline](#)
51. Shi, Y., Suh, Y. H., Milstein, A. D., Isozaki, K., Schmid, S. M., Roche, K. W., and Nicoll, R. A. (2010) Functional comparison of the effects of TARPs and cornichons on AMPA receptor trafficking and gating. *Proc. Natl. Acad. Sci. U. S. A.* **107**, 16315–16319 [CrossRef Medline](#)
52. Eggington, J. M., Greene, T., and Bass, B. L. (2011) Predicting sites of ADAR editing in double-stranded RNA. *Nat. Commun.* **2**, 319 [CrossRef Medline](#)
53. Bordoli, L., Kiefer, F., Arnold, K., Benkert, P., Battey, J., and Schwede, T. (2009) Protein structure homology modeling using SWISS-MODEL workspace. *Nat. Protoc.* **4**, 1–13 [CrossRef Medline](#)